

# Experimental Investigation on Deformation Failure Characteristics of Crystalline Marble Under Triaxial Cyclic Loading

Sheng-Qi Yang<sup>1</sup> · Wen-Ling Tian<sup>1</sup> · P. G. Ranjith<sup>1,2</sup>

Received: 12 February 2017 / Accepted: 8 June 2017 / Published online: 6 July 2017  
© Springer-Verlag GmbH Austria 2017

**Abstract** The deformation failure characteristics of marble subjected to triaxial cyclic loading are significant when evaluating the stability and safety of deep excavation damage zones. To date, however, there have been notably few triaxial experimental studies on marble under triaxial cyclic loading. Therefore, in this research, a series of triaxial cyclic tests was conducted to analyze the mechanical damage characteristics of a marble. The post-peak deformation of the marble changed gradually from strain softening to strain hardening as the confining pressure increased from 0 to 10 MPa. Under uniaxial compression, marble specimens showed brittle failure characteristics with a number axial splitting tensile cracks; in the range of  $\sigma_3 = 2.5\text{--}7.5$  MPa, the marble specimens assumed single shear fracture characteristics with larger fracture angles of about  $65^\circ$ . However, at  $\sigma_3 = 10$  MPa, the marble specimens showed no obvious shear fracture surfaces. The triaxial cyclic experimental results indicate that in the range of the tested confining pressures, the triaxial strengths of the marble specimens under cyclic loading were approximately equal to those under monotonic loading. With the increase in cycle number, the elastic strains of the marble specimens all increased at first and later decreased,

achieving maximum values, but the plastic strains of the marble specimens increased nonlinearly. To evaluate quantitatively the damage extent of the marble under triaxial cyclic loading, a damage variable is defined according to the irreversible deformation for each cycle. The evolutions of the elastic modulus for the marble were characterized by four stages: material strengthening, material degradation, material failure and structure slippage. Based on the experimental results of the marble specimens under complex cyclic loading, the cohesion of the marble decreased linearly, but the internal friction angles did not depend on the damage extent. To describe the peak strength characteristics of the marble specimens under complex cyclic loadings with various deformation positions, a revised strength criterion for damaged rocks is offered.

**Keywords** Crystalline marble · Mechanical damage · Elastic modulus · Strength · Cyclic loading

## 1 Introduction

Due to the influence of disturbances from strong blasting and excavation in all kinds of rock engineering, rock masses often experience cyclic loading, which leads to the continuous damage and failure of tunnels (Zhu et al. 2010; Xu et al. 2012; Zhou et al. 2012; Zhou and Zhang 2017). Previous experimental studies have demonstrated that the mechanical behaviors of rocks under cyclic loading are significantly different from those under monotonic loading (Rao and Ramana 1992; Bagde and Petros 2005; Heap et al. 2009a, b; Wang et al. 2013; Yang et al. 2015a). Therefore, it is very important to investigate the mechanical damage characteristics of rock subjected to cyclic

✉ Sheng-Qi Yang  
yangsqi@hotmail.com

<sup>1</sup> State Key Laboratory for Geomechanics and Deep Underground Engineering, School of Mechanics and Civil Engineering, China University of Mining and Technology, Xuzhou 221116, People's Republic of China

<sup>2</sup> Deep Earth Energy Research Laboratory, Department of Civil Engineering, Monash University, Melbourne, VIC 3800, Australia

loading to better understand the unstable failure mechanisms encountered in rock engineering.

Using ultrasonic and acoustic emission (AE) monitoring techniques, Rao and Ramana (1992) investigated the progressive failure characteristics of granite under uniaxial cyclic loading. Akesson et al. (2004) and Xiao et al. (2010) investigated the damage failure characteristics of granite under uniaxial cyclic loading and analyzed the relation between damage variable and cycle number. Wang et al. (2013) examined the fatigue behavior of granite under triaxial cyclic loading by performing a series of laboratory tests. The results showed that the axial residual strain decreased with cycle number when the peak deviatoric stress was less than the threshold for fatigue failure, whereas the axial residual strain increased with cycle number when the maximum stress was higher than the threshold. Erarslan and Williams (2012) presented experimental results of strength and deformation behaviors of Brisbane tuff disk specimens under indirect cyclic tension. Their results showed that a macroscale splitting crack with a sharp and rough surface was found along the diametric compressive direction under monotonic loading, whereas an excessive amount of small particles and dust was produced under cyclic loading. Liu et al. (2014) conducted uniaxial cyclic tests to investigate the damage evolution of rock salt. The results showed that the stress levels leading to the initiation and accelerated accumulation of fatigue damage under the cyclic loading process were between 20 and 40% of the uniaxial compressive strength (UCS) of the tested rock salt. In addition, shear testing is used to investigate the mechanical behaviors of rocks under cyclic shear loading. In accordance with shear test results on rock joints under cyclic loading, Jafari et al. (2003) found that the shear strength of joints depended not only on shearing velocity, but also on the number of loading cycles and stress amplitude. Yang et al. (2015a) reported on a series of triaxial cyclic experimental results on sandstone under different confining pressures. These researchers compared triaxial monotonic and cyclic mechanical parameters of sandstone specimens under different confining pressures and analyzed the influence of cycle number on the crack damage threshold of sandstone. Furthermore, they explored the internal damage characteristics of a sandstone material after triaxial monotonic and cyclic failure using an X-ray micro-CT scanning system.

Marble, a type of metamorphic rock, is ubiquitous in all kinds of rock engineering. Yang et al. (2008) carried out a conventional triaxial compression experiment investigation for marble with two preexisting closed cracks with non-overlapping geometries by fixing the flaw and ligament lengths. The experimental results showed that intact and flawed marbles had different deformation properties after peak stress. The peak strength and failure

mode were found to depend not only on flaw geometry, but also on confining pressure. Yang et al. (2011) designed three complex loading paths to investigate the re-fracture mechanical behavior of flawed coarse marble. They found that the peak strength and deformation failure mode of the flawed coarse marble depended on the loading paths. They then analyzed the effects of complex loading paths on strength, deformation and failure behavior of the flawed coarse marble under different confining pressures. Pei et al. (2016) carried out uniaxial compression experiments with acoustic emission (AE) monitoring on marble specimens containing natural fractures. They analyzed the characteristics of the AE events and spatial evolution of fractures in marble specimens containing various types of natural fractures, which revealed the crack propagation processes by the spatial evolutions of the AE events. Migliazza et al. (2011) compared the results of static and cyclic experimental tests on Carrara marble. They evaluated fatigue strength and estimated fatigue crack growth rate. Qiu et al. (2014) proposed an incrementally cyclic loading–unloading press test to quantify stress-induced microfracturing and fracturing in marble under a condition of reductions in confining pressure. The experimental results demonstrated pre-peak damage, and deformation characteristics of the marble specimens could be easily quantified by irreversible strains. Two damage stages, namely a linear steady stage and a nonlinear unsteady stage, which were, respectively, represented using linear steady rate and nonlinear unsteady rates of damage evolution, occurred along with increasing unloading damage. In accordance with short-term triaxial experimental results for marble under cyclic loading, Yang et al. (2015b) investigated the elastic, plastic and strength behaviors of marble. The experimental results showed that for the same confining pressures, the elastic modulus of the marble remains constant at a lower axial deviatoric level but decreased slowly after yielding strength. However, the plastic modulus of the marble decreased rapidly with increasing axial deviatoric stress at the same confining pressure. Moreover, the elastic and plastic moduli of the tested marble were independent of confining pressure.

Therefore, in this paper, we report the results of a series of triaxial monotonic and cyclic compression tests on marble under different confining pressures. Based on the experimental results of the marble under triaxial monotonic loading, the effect of confining pressure on the strength and deformation failure behavior of the marble specimens is first compared. Using the experimental results of the marble under triaxial cyclic loading, the influence of cycle number on the strain damage behavior and elastic modulus of the marble is analyzed. Finally, on the basis of the experimental results of the marble under complex cyclic

loading, the strength and deformation parameters of the marble specimens with various damage extents are evaluated.

## 2 Marble and Testing Procedure

### 2.1 Marble Material and Specimen Preparation

The material used throughout this research was marble collected from Guilin city in Guangxi Province, China. The marble material has a connected porosity of 0.57% and an average unit weight of approximately 2680 kg/m<sup>3</sup>. According to X-ray diffraction (XRD) test results, the marble material consisted mainly (98.6%) of carbonate minerals (calcite) and fewer clay minerals (1.4%). The marble had a crystalline and blocky structure (Fig. 1), which is macroscopically very homogenous. In this experiment, all the specimens were cored from the same block of material to an actual diameter of 50 mm and approximate 100 mm in length. All the experiments were performed on dry

specimens at room temperature. Table 1 lists the tested marble specimens and conditions in this research.

The triaxial experiments on the marble specimens were all carried out with rock servo-controlled triaxial equipment (Fig. 2) (Yang et al. 2014). The equipment included a loading system, constant-stability pressure equipment, a hydraulic pressure transfer system, a pressure chamber, a hydraulic pressure system and an automatic data collection system. The most important part of the equipment was the self-equilibrium triaxial pressure chamber system, which was comprised of three high-precision pumps that controlled axial pressure (P1), confining pressure (P2) and pore pressure (P3, P4). The maximum capacities of P2 and pore pressure (P3 = P4) were 60 MPa. However, the maximum capacity of P1 was as high as 400 MPa for a normal cylindrical specimen with a diameter of 50 mm. When testing, the axial displacement was measured using two linear variable differential transformers (LVDTs) that were fixed between the bottom and top surfaces of the specimen inside the triaxial cell.

**Fig. 1** Microscopic structure of marble used in this research. **a** Sampling location; **b** optical microscopy; and **c** SEM photograph

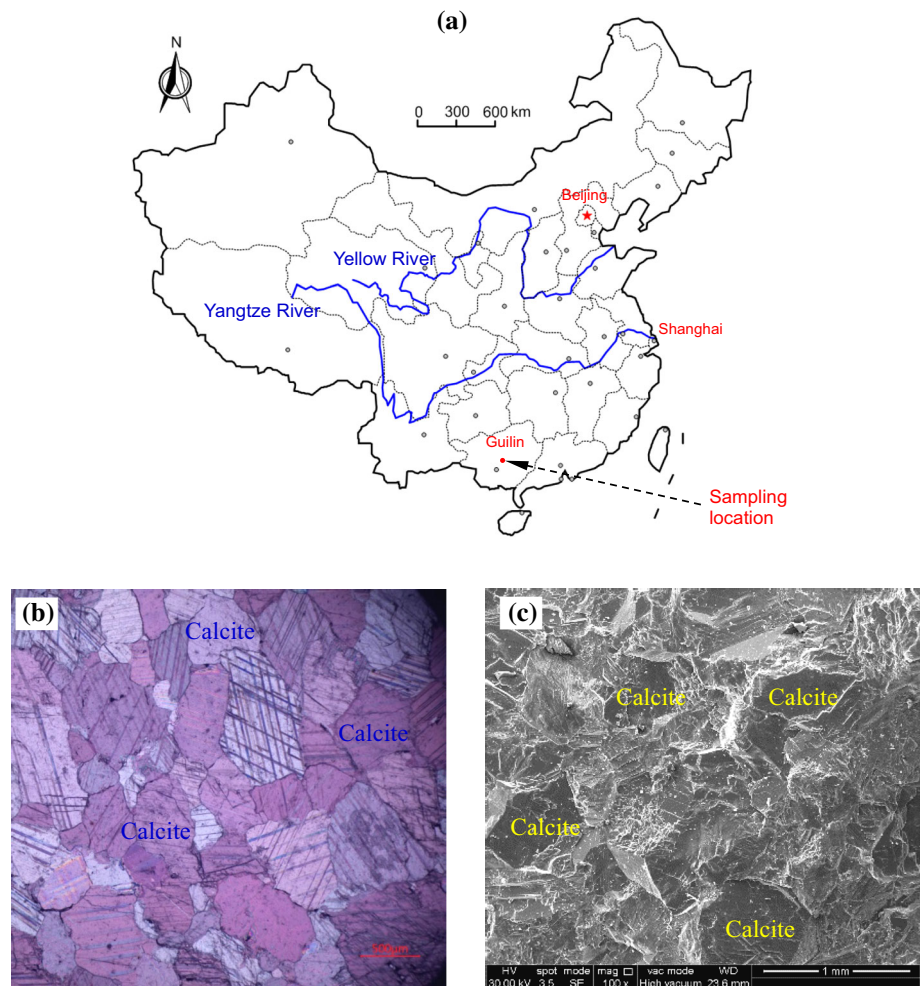


**Table 1** Tested marble specimens and conditions in this research

Specimen	$D$ (mm)	$L$ (mm)	$M$ (g)	$\rho$ (kg/m <sup>3</sup> )	$\sigma_3$ (MPa)	Note
GL-A1 <sup>#</sup>	49.90	100.80	530.81	2692.7	0	Triaxial monotonic loading
GL-A3 <sup>#</sup>	49.90	100.82	530.39	2690.0	0	Triaxial monotonic loading
GL-A4 <sup>#</sup>	49.98	100.90	530.48	2679.8	5	Triaxial monotonic loading
GL-A5 <sup>#</sup>	50.00	100.94	531.18	2680.1	10	Triaxial monotonic loading
GL-A6 <sup>#</sup>	49.96	100.68	527.06	2670.4	2.5	Triaxial monotonic loading
GL-A7 <sup>#</sup>	49.98	100.76	529.64	2679.2	7.5	Triaxial monotonic loading
GL-A8 <sup>#</sup>	50.00	100.70	529.64	2687.7	2.5	Simple cyclic loading
GL-A9 <sup>#</sup>	49.96	100.88	531.35	2686.8	5	Simple cyclic loading
GL-A10 <sup>#</sup>	49.98	100.38	528.93	2685.8	7.5	Simple cyclic loading
GL-A11 <sup>#</sup>	49.98	100.38	527.39	2677.9	10	Simple cyclic loading
GL-A12 <sup>#</sup>	50.00	100.06	527.56	2685.2	10–2.5–5.0–7.5–10	Complex cyclic loading
GL-A13 <sup>#</sup>	49.96	100.88	528.06	2670.2	10–2.5–5.0–7.5–10	Complex cyclic loading
GL-A14 <sup>#</sup>	49.98	100.40	527.63	2678.6	10–2.5–5.0–7.5–10	Complex cyclic loading
GL-A16 <sup>#</sup>	50.00	100.40	533.32	2705.4	10–2.5–5.0–7.5–10	Complex cyclic loading
GL-A17 <sup>#</sup>	50.00	100.80	529.86	2677.1	10–2.5–5.0–7.5–10	Complex cyclic loading

$D$  diameter,  $L$  length,  $\rho$  density,  $M$  mass,  $\sigma_3$ , confining pressure

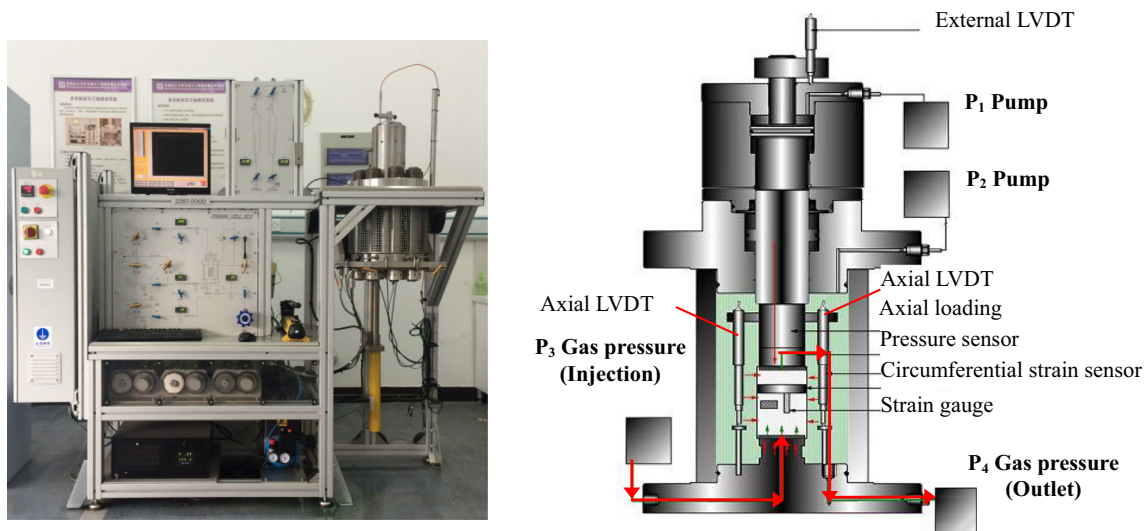


**Fig. 2** Rock servo-controlled triaxial equipment (modified from Yang et al. 2014)

## 2.2 Two Types of Triaxial Tests

To investigate the evolution of the mechanical damage of the marble material, we performed two types of triaxial tests: (1) monotonic and (2) cyclic.

The triaxial monotonic experiments (Fig. 3) (i.e., the conventional triaxial experiment) were carried out under different confining pressures ( $\sigma_3$ ) of 2.5, 5.0, 7.5 and 10 MPa and consisted of the following two steps. First, the confining pressure was increased to the desired value at a constant rate of 0.1 MPa/s to ensure that the specimen was under uniform hydrostatic stresses. The deviatoric stress ( $\sigma_1 - \sigma_3$ ) was then applied to the surface of the specimen at a constant axial displacement rate of 0.02 mm/s until failure.

In Fig. 3,  $\varepsilon_1$  represents the axial strain and  $\sigma_1$  represents major principal stress.

The triaxial cyclic experiments can be divided into two groups. The first group is triaxial cyclic loading, which was conducted using the following three steps. First, the hydrostatic pressure was applied to the specimens at a rate of 0.1 MPa/s until the desired values were reached. Second, the specimens were loaded to the first displacement value (corresponding to the first deviatoric stress level) at a controlled axial displacement rate of 0.02 mm/s, and the first deviatoric stress level was then unloaded to zero at a rate of 0.4 MPa/s through controlling axial force. In each subsequent cycle, the second deviatoric stress level was increased, and the specimens were again unloaded to zero.



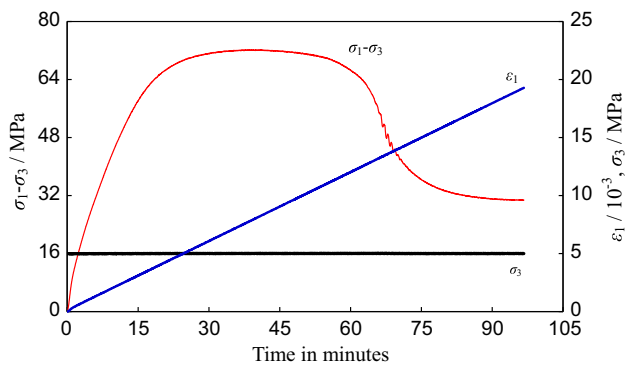


**Fig. 3** A typical experimental result of triaxial monotonic loading path on marble specimen. The blue line represents the axial strain, the black line represents the confining pressure, and the red line represents the axial deviatoric stress (color figure online)

Finally, the stress cycling was continued in that way until the specimens eventually failed. It should be noted that in our study, after peak strength, multiple cyclic loadings were continued to analyze the mechanical behaviors of the fractured rock material, a procedure unlike that used in previous studies (Heap et al. 2009b; Trippetta et al. 2013). Figure 4 shows a typical experimental result of triaxial cyclic loading path for a marble specimen that failed at the 11th loading cycle.

The second group is complex cyclic loading (Yang and Jing 2013), which was conducted with the following steps. First, a hydrostatic pressure of 10 MPa was applied to the specimens at a rate of 0.1 MPa/s. Second, the specimens were loaded to the first displacement value, i.e., point A shown in Fig. 5 (note: this displacement value of point A can be designed before or after peak strength) at a controlled axial displacement rate of 0.02 mm/s, and the deviatoric stress level was then unloaded to zero at a rate of 0.4 MPa/s through controlling axial force. Maintaining a

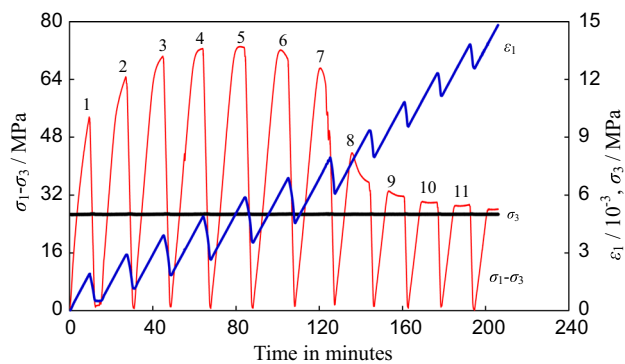


**Fig. 4** A typical experimental result of simple cyclic loading path from increasing amplitude, cyclic stressing triaxial experiment on marble specimen. The numbers in this figure represent the cycle number. The blue line represents the axial strain, the black line represents the confining pressure, and the red line represents the axial deviatoric stress (color figure online)

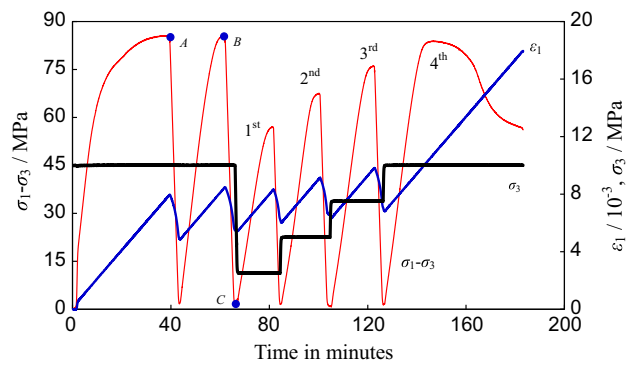


**Fig. 5** A typical experimental result of complex cyclic loading path from increasing amplitude, cyclic stressing triaxial experiment on marble specimen. The blue line represents the axial strain, the black line represents the confining pressure, and the red line represents the axial deviatoric stress (color figure online)

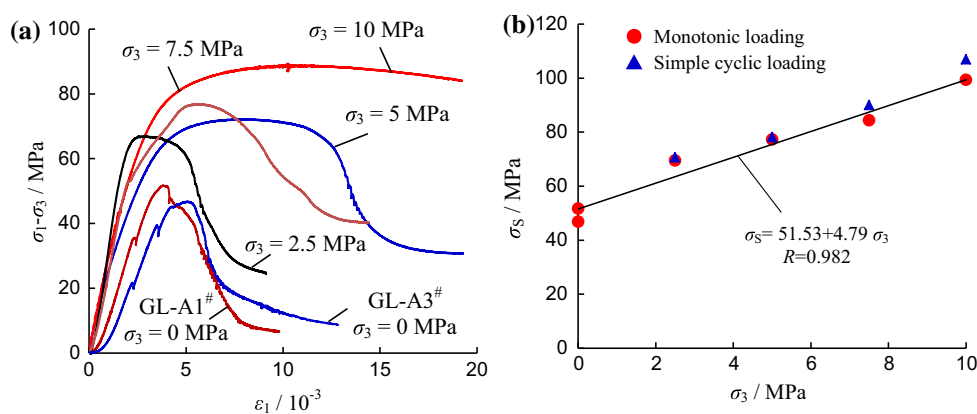
constant 10 MPa confining pressure, the specimens were reloaded to point B at a controlled axial displacement rate of 0.02 mm/s. Afterward, the deviatoric stress level was unloaded to zero (point C) at a controlled axial force of 0.4 MPa/s.

At that time, the 10 MPa confining pressure was reduced to 2.5 MPa (1st stage) at a rate of 0.1 MPa/s. The deviatoric stress was loaded at a constant axial displacement control rate of 0.02 mm/s until the specimen reached post-failure, at which point, the deviatoric stress dropped by ~2% from its peak. The confining pressure was then hydrostatically increased to the 2nd stage, i.e., 5.0 MPa. After that, the preceding steps were repeated at the third confining pressure (3rd stage), 7.5 MPa. At the fourth confining pressure (4th stage) of 10 MPa, the deviatoric stress was loaded to the surface of the specimens at a constant axial displacement control rate of 0.02 mm/s until failure occurred. Thus, we were able to obtain a series of peak strengths of the damaged specimens under different confining pressures. Figure 5 shows a typical experimental result of complex cyclic loading path for a marble specimen.

### 3 Experimental Results of Marble Under Triaxial Monotonic Loading

The deviatoric stress–axial strain curves for the marble under different confining pressures are presented in Fig. 6a. According to Fig. 6a, the post-peak deformation of the marble changed gradually from strain softening to strain hardening with increasing confining pressure. When  $\sigma_3$  equals ~10 MPa, the deformation of the marble specimen shows a distinct yielding platform and plastic flow occurs, i.e., the post-peak deformation behavior of the specimen changes into ideal plasticity. The above brittle–ductile

**Fig. 6** Experimental results of marble specimens under triaxial monotonic loading. **a** Deviatoric stress–axial strain curves of marble specimen under different confining pressures; **b** comparison of monotonic and simple cyclic triaxial strength of marble specimen under different confining pressures



transition of the marble is also approximate to the previous findings for Jinping marble (Yang et al. 2016).

On the basis of the peak strength values shown in Fig. 6a, the influence of  $\sigma_3$  on the peak strength of the marble is presented in Fig. 6b. Figure 6b indicates that the peak strength of the marble showed distinctly linear behavior with increasing  $\sigma_3$ , in good agreement with the linear Mohr–Coulomb criterion, i.e., Eq. (1):

$$\sigma_S = \sigma_0 + q\sigma_3 = \frac{2C \cos \varphi + \sigma_3(1 + \sin \varphi)}{1 - \sin \varphi} \quad (1)$$

where  $\sigma_S$  is the maximum axial supporting capacity of the rock,  $\sigma_0$  is usually regarded as the uniaxial compressive strength (UCS) of rock material, and  $q$  is an influence coefficient of the confining pressure on  $\sigma_S$  of the rock. The  $\sigma_0$  and  $q$  are related to the cohesion  $C$  and internal friction angle  $\varphi$  of the rock material.

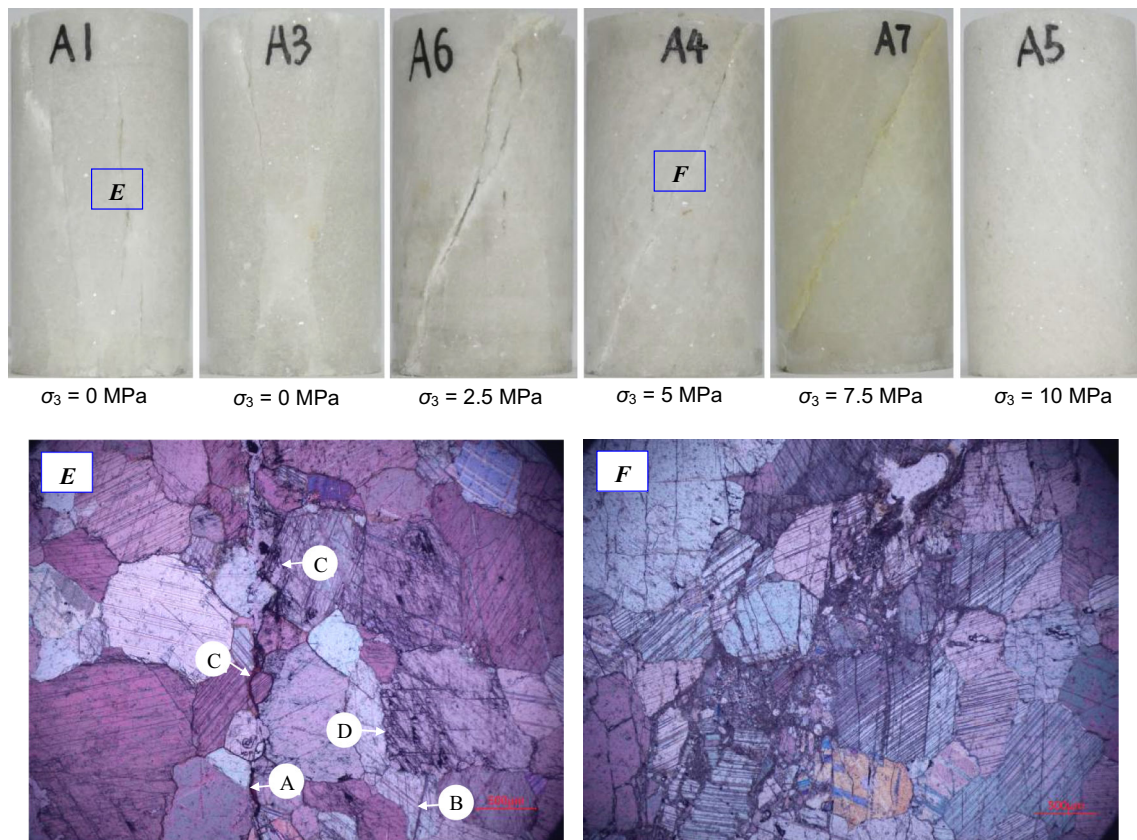
By using the linear Mohr–Coulomb criterion, the peak strength parameters of the marble under triaxial monotonic loading can be calculated. We determined that the cohesion of the marble was 11.77 MPa, and the internal friction angle was 40.9°.

Figure 7 shows the ultimate failure modes of the marble specimens under triaxial monotonic loading. From Fig. 7, we can see that the marble specimens experienced some axial splitting tensile cracks, which validates the brittle failure of the marble material under uniaxial compression and was also approximately that of previous findings on Jinping marble (Yang et al. 2016). Furthermore, specimens A1# and A3# exhibited some differences, even though both displaying the tensile fracture modes, which resulted from the influence of rock heterogeneity on the fracture characteristics. However, at confining pressures of 2.5–7.5 MPa, the marble specimens mainly failed by shear localization along an inclined macroscopic shear band with a single shear zone across each specimen. The shear fracture angle was approximately 65°, which was approximately equal to  $45^\circ + \varphi/2$ . Furthermore, the fracture angles did not depend on confining pressure at

$\sigma_3 = 2.5$ –7.5 MPa. However, at  $\sigma_3 = 10$  MPa, no obvious shear fracture surfaces could be observed by the unaided eye, which is also evidenced by the axial deviatoric stress–axial strain curve shown in Fig. 6a.

To analyze the deformation mechanism of the marble specimen after triaxial monotonic loading failure, an optical microscope is used to observe the microscopic characteristics of failed marble specimen. The previous research for Carrara marble (Cheng et al. 2016) has verified that the optical observation is favored for identifying grain boundaries and cracks because the different grains will show a different degree of grayish color and open cracks will remain black under optical microscope. Two square regions shown in Fig. 7 will be chosen to perform the microscopic examination, since a lot of serious damage has occurred in these regions. To avoid any possible additional damage associated with saw cutting, a dye epoxy was used to fill the flaws and newly developed microcracks and strengthened the failed specimens. A large amount of polishing was carried out to form a better thin section.

Figure 7 also shows microscopic observation results of a marble specimen after triaxial monotonic loading failure with respect to  $\sigma_3 = 0$  and 5 MPa. Compared with the microscopic observation results of the uncompressed marble specimen shown in Fig. 1a, it is clear that the local damage failure of the marble specimen after triaxial monotonic loading obviously differed, depending on the confining pressure. A further analysis can be illustrated as follows. It can be seen that under uniaxial compression, tensile cracks were observed along the direction of the major principal stress. In the previous research (Cheng et al. 2016), four principal nucleation mechanisms for transgranular cracks were observed in Carrara marble subjected to uniaxial compression loading. Type A and Type B mechanisms were favored by the distinctive polygonal shapes of the crystal grains in the marble. The local tensile stress concentration in those two mechanisms is attributed to grain sliding and divergent normal contact force, respectively. The Type C mechanism is associated



**Fig. 7** Ultimate failure mode and photomicrographs of marble specimen under triaxial monotonic loading. Type A and Type B mechanisms were favored by the distinctive polygonal shapes of the crystal grains in the marble, the Type C mechanism is associated with

with gliding along twin lamellae, and the Type D mechanism operates in grains that failed mainly due to compressive stress rather than tensile stress concentrations. The above four mechanisms were also observed for our marble specimens under uniaxial compression, as shown in Fig. 7. However, at confining pressures of 5 MPa, the nucleation mechanism in the marble differed from that under uniaxial compression. It is clear that at  $\sigma_3 = 5$  MPa, shear slippage was very obvious; furthermore, different regions showed various damage extents.

#### 4 Triaxial Experimental Results of Marble Under Simple Cyclic Loading

Figure 8 shows typical triaxial experimental results for the marble specimens under simple cyclic loading at  $\sigma_3 = 2.5, 5, 7.5$  and 10 MPa. It should be noted that even after the peak stress, the specimens still continued to undergo cyclic loading until the residual strength, which occurred easily due to ductile failure of the marble material after peak strength.

gliding along twin lamellae, and the Type D mechanism operates in grains that failed mainly due to compressive stress rather than tensile stress concentrations (Cheng et al. 2016)

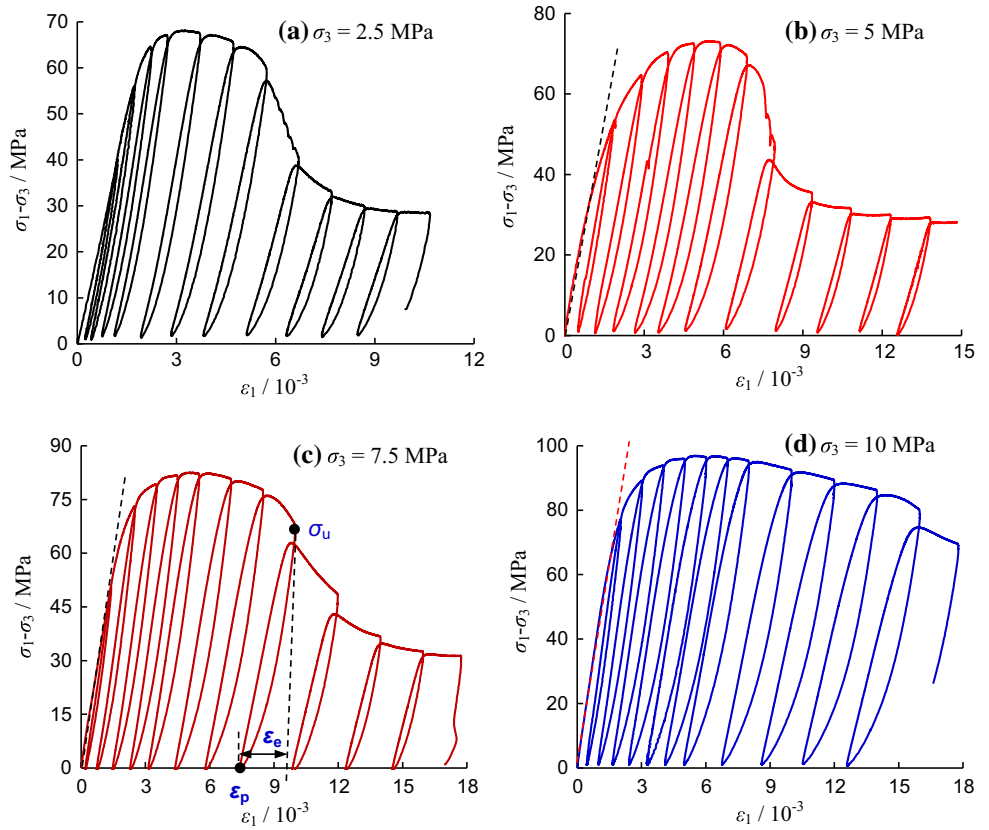
Based on the triaxial experimental results of the marble under monotonic and simple cyclic loading shown, respectively, in Figs. 6a and 8, the comparison of the peak strengths under monotonic and simple cyclic loading is presented in Fig. 6b. From Fig. 6b, we can see that the cyclic triaxial strength of the marble was approximately equal to the monotonic triaxial strength, which indicates that in the range of the tested confining pressures, cyclic loading did not affect the triaxial strength of the marble compared with monotonic loading.

In accordance with Fig. 8, we confirmed the elastic and plastic deformations (irreversible deformation) of marble specimens for each loading–unloading cycle. The  $\epsilon_e, \epsilon_p$  and  $\sigma_u$  are defined the elastic strain, plastic strain and unloading deviatoric stress level of rock, respectively, as depicted in Fig. 8c.

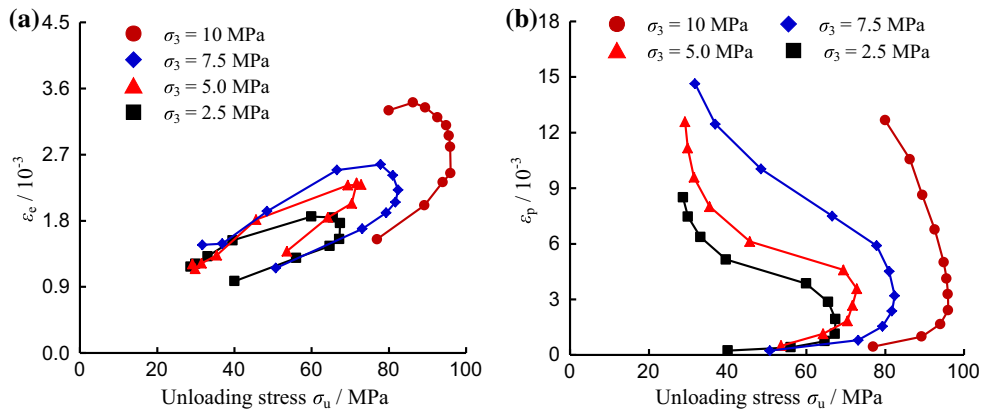
##### 4.1 Effect of Cyclic Number and Unloading Stress Level on the Strain Behavior of Marble

Figure 9 illustrates the relationship between unloading stress level and the strains of the marble specimens under

**Fig. 8** Triaxial experimental results of marble specimens under simple cyclic loading in accordance with the path shown in Fig. 4



**Fig. 9 a** Relationship between elastic strain and unloading stress level; **b** relationship between plastic strain and unloading stress level



different confining pressures. From Fig. 9a, it can be seen that with the increase in unloading stress level, the elastic deformation of the marble also increased gradually before peak strength; furthermore, that variance did not depend obviously on confining pressure. However, after peak strength, the relationship between unloading stress level and the strains of the marble specimens depended on the confining pressure. At  $\sigma_3 = 5.0$  MPa, after the peak strength, the elastic deformations of the marble specimens decreased with the decreases in the unloading stress levels. However, at  $\sigma_3 = 2.5, 7.5$  and  $10$  MPa, after the peak strength, the elastic deformations of the marble specimens

first increased gradually and then decreased with the decreasing unloading stress level.

Figure 9b illustrates the effects of unloading stress levels on the plastic deformation of the marble under different confining pressures, which were obviously unlike those of the elastic deformation of the marble shown in Fig. 9a. For the same confining pressure, and at early several cyclic stress levels, the elastic deformation of the marble exceeded the plastic deformation, but afterward, the plastic deformation of the marble was higher than the elastic deformation, which was a result of the increased number of cycles, whereby the specimens experienced



increasingly greater crack damage, which resulted in an increasing amount of irreversible deformation. It should be noted that the plastic deformation of the marble increased slowly as unloading stress level increased, whereas after the peak strength, the plastic deformation of marble increased dramatically, despite the reduction in unloading stress level. The rate of plastic deformation increased with applied confining pressure.

Figure 10 shows the relationship between cycle number and strains for the marble specimens under different confining pressures. From Fig. 10a, we can see that with the increase in cycle number, the elastic strains for the marble specimens at first increased and then decreased, and all had maximum values. However, the cycle numbers corresponding to the maximum elastic strain values of the marble specimens differed for various confining pressures. From Fig. 10b, it can be seen that the plastic strains of the marble specimens increased nonlinearly with cycle number.

Figure 11 shows the comparison of elastic and plastic strains of marble at the same confining pressure. From Fig. 11, we can see that in lower cycle number, the elastic strain of the marble specimens was slightly higher than the plastic strain for the same confining pressure. However, in higher cycle number, the elastic strain of the marble specimen was obviously lower than the plastic strain for the same confining pressure. Furthermore, with the increase in cycle number, the difference between the elastic and plastic strain increased gradually.

To quantitatively evaluate the damage extent of the marble specimens under triaxial cyclic loading, a damage variable is defined in accordance with the irreversible deformation (plastic deformation) for each cycle (Yang et al. 2015a) and is expressed in Eq. (2):

$$D = \frac{(\epsilon_p)_N}{\sum_{N=1}^m (\epsilon_p)_N} \tag{2}$$

where  $D$  represents the damage variable of rock.  $\epsilon_p$  represents the irreversible deformation of rock, and  $N$  is the

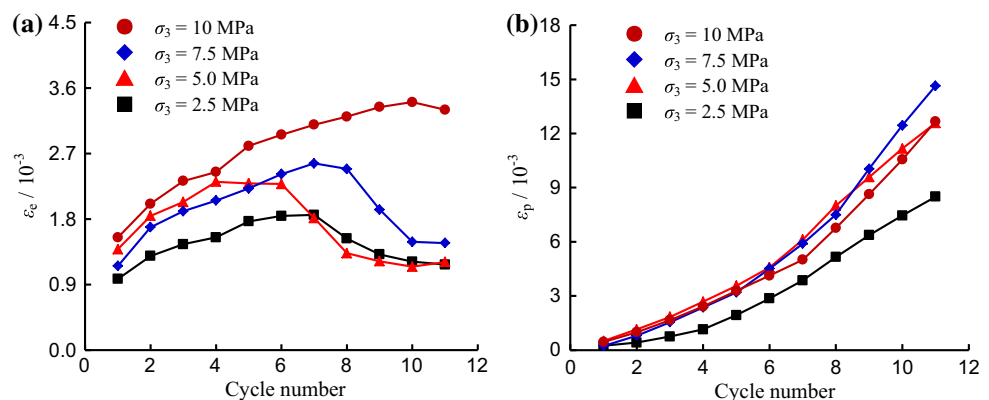
cycle number. The letter  $m$  represents the maximum cycle number.

Figure 12 shows the damage evolution of the marble specimens under different confining pressures. From Fig. 12, it is clear that the confining pressure had almost no effect on the damage evolution of the marble specimens. However, at the same confining pressure, the damage variable values of the marble specimens increased with increasing cycle number. Furthermore, the extent of the damage variable increased with increasing cycle number.

### 4.2 Evolution of Elastic Modulus of Marble with Cyclic Number

The evolution of elastic modulus of marble can be characterized as having four stages (Fig. 13): (a) Stage I: material strengthening; (b) Stage II: material degradation; (c) Stage III: shear failure; and (d) Stage IV: structure slippage. At  $\sigma_3 = 2.5, 5.0$  and  $7.5$  MPa, the above four stages were very obvious. During Stage I, the elastic modulus ( $E$ ) of the marble increased obviously, which indicates that the marble became stiffer and more difficult to deform. In our research, the unloading stress levels of the marble specimens for the first cycle were located at the stage of yielding before peak strength. The reason for the evolution can be presented as follows. With the increase in cycling stress, some mesoscopic elements with lower strengths and stiffnesses first reached their maximum supporting capacities, yield softening, and produced plastic deformation as the specimens yielded (Yang et al. 2008). Some extruded and fractured elements then filled the internal voids of the marble specimens. On the other hand, preexisting pores and fissures could also produce closure. The above two factors strengthened the supporting structure of the marble material, which resulted in the increase in  $E$ . During Stage II, we observe a significant decrease in  $E$ . At  $\sigma_3 = 2.5$  MPa, the elastic modulus decreased from 44.73 to 32.95 GPa during increasing amplitude cycling stressing to failure. At  $\sigma_3 = 5.0$  MPa, the elastic modulus

**Fig. 10** a Relationship between elastic strain and cycle number; b relationship between plastic strain and cycle number



**Fig. 11** Comparison of elastic and plastic strains of marble at the same confining pressure

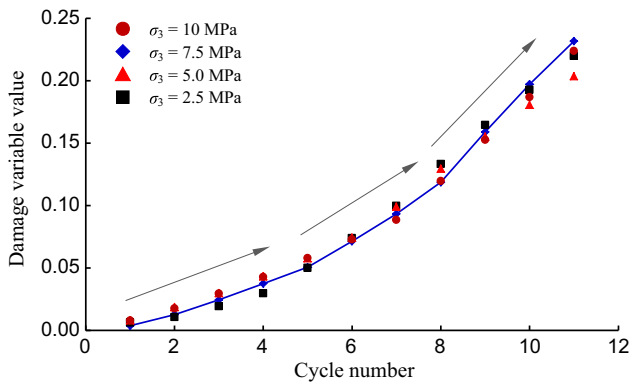
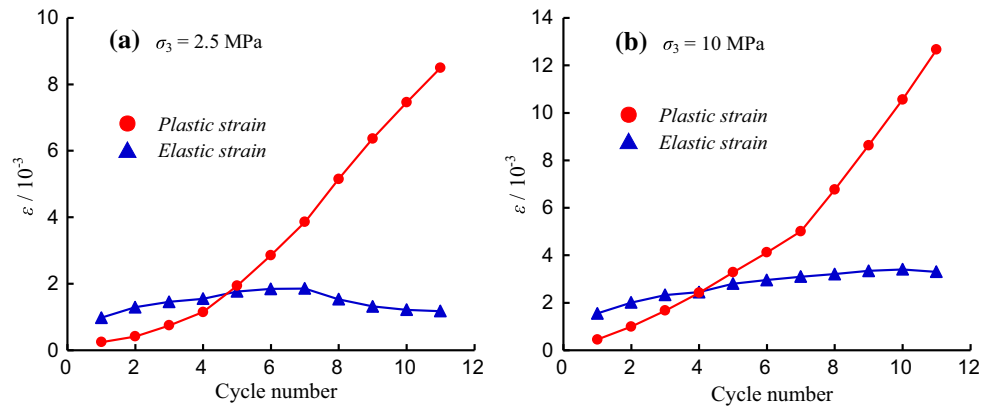
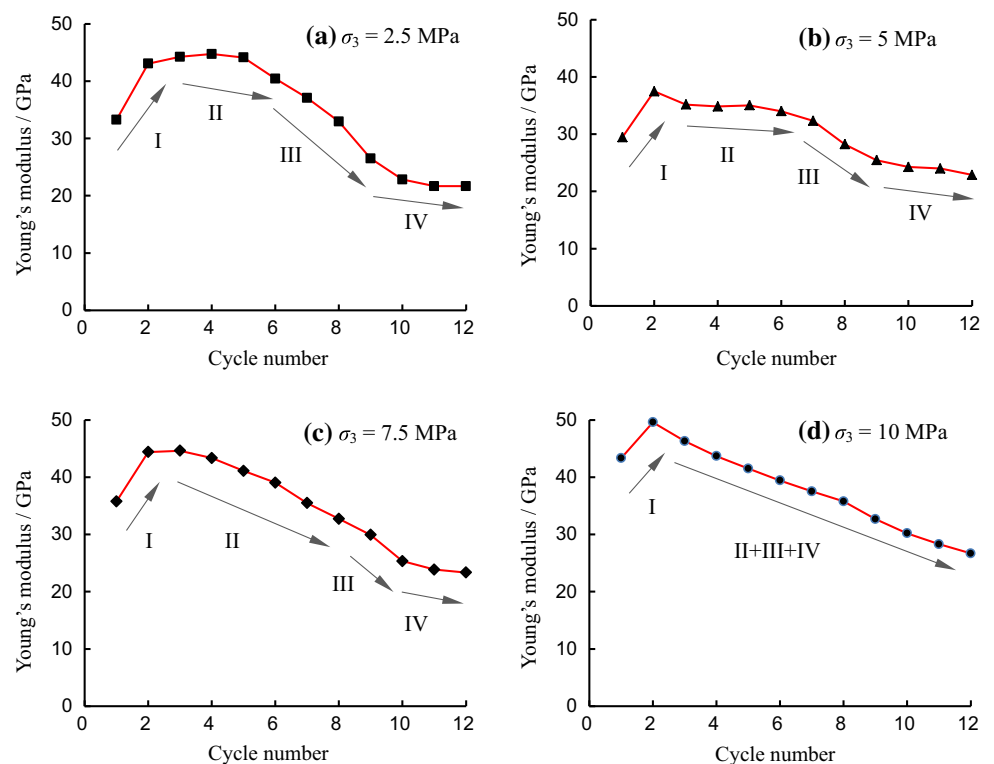


**Fig. 12** Relationship between cycle number and damage variable value of marble under different confining pressures

decreased from 37.48 to 32.33 GPa during increasing amplitude cycling stressing to failure. At  $\sigma_3 = 7.5$  MPa, the elastic modulus decreased from 44.63 to 32.73 GPa during increasing amplitude cycling stressing to failure. The decrease in  $E$  can be attributed to a progressive degradation in the stiffness of the rock due to the increase in crack damage with increasing cycle number. At higher stress levels, each cycle applied to a specimen will produce an additional increment in crack damage, resulting in an increasing amount of irreversible deformation. During Stage III, it is very clear that the elastic modulus of marble specimen decreased. At  $\sigma_3 = 2.5$  MPa, the elastic modulus decreased significantly from 32.95 to 22.82 GPa during this stage. At  $\sigma_3 = 5.0$  MPa, the elastic modulus decreased

**Fig. 13** Evolution of elastic modulus of marble specimens with the increase in cycle number under various confining pressures



from 32.33 to 24.26 GPa during this stage. At  $\sigma_3 = 7.5$  MPa, the elastic modulus decreased from 32.73 to 25.33 GPa during this stage. The variance in  $E$  for the marble specimens during this stage can be explained as follows. During this stage, larger macroscopic cracks will have formed, resulting in the failure of the structure of the rock material. Therefore, the increase in the number of macroscopic cracks reduces axial stiffness. During Stage IV, the elastic modulus decreased slightly from 22.82 to 21.66 GPa at  $\sigma_3 = 2.5$  MPa. The elastic modulus changed from 24.26 to 22.88 GPa at  $\sigma_3 = 5.0$  MPa. At  $\sigma_3 = 7.5$  MPa, the elastic modulus changes from 25.33 to 23.35 GPa. This indicates that the elastic modulus of the marble is dependent on cycle number during this stage, which results from the following reason. Due to the constriction of confining pressure, the specimens had entered the stage of residual strength and mainly supported the axial capacity by friction slippage in the macroscopic failure plane, which resulted in no obvious variance in the  $E$  of the marble specimens.

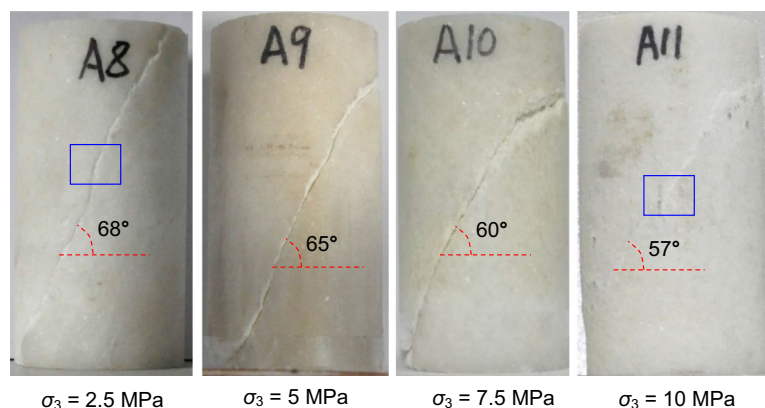
However, at  $\sigma_3 = 10$  MPa, the above Stages II, III and IV could only be distinguished with great difficulty, as shown in Fig. 13d. This can be explained as follows. Under the confining pressure, after the first cycle, with the increase in axial deformation, the mesoscopic material elements with low strength and stiffness first reached their maximum supporting capacities, experienced yield softening and produced the plastic deformation. Afterward, if we want the specimen to fail macroscopically, the axial stress must be increased continuously. Thus, when the macroscopic stress–strain response of the tested marble specimens reached the peak stress, the mesoscopic material elements with higher strengths and stiffnesses in the specimens also reached their maximum supporting limits, yielding failure and initiating plastic deformation. Therefore, the total deformations in the specimens would tend to be uniform, and the plastic deformations of the specimens would also increase with cycle number, as shown in Fig. 10d, which results in distinct yielding platform in the

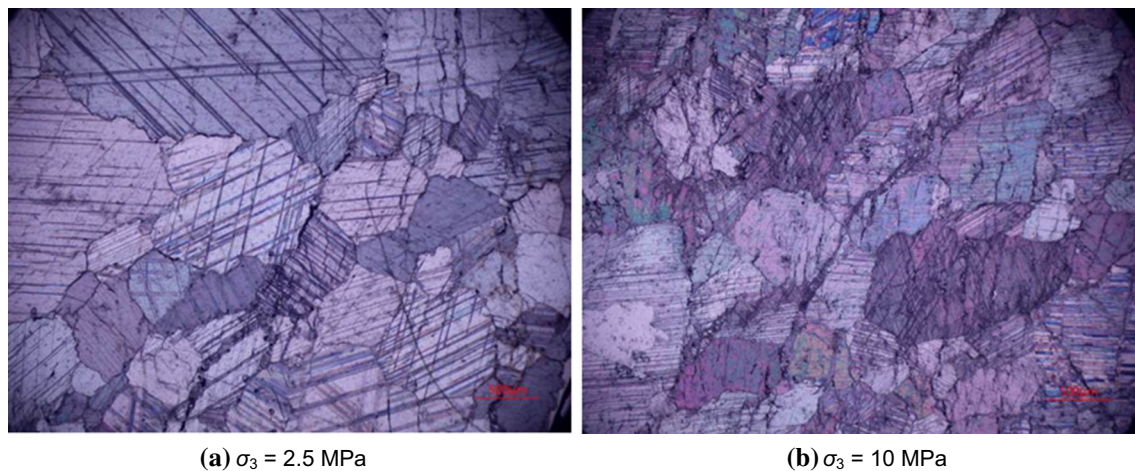
macroscopic stress–strain curves near the peak stress, as shown in Fig. 8d. Therefore, the three stages II, III and IV are very difficult to distinguish.

Figure 14 depicts the ultimate failure mode of the marble specimens under simple cyclic loading. From Fig. 14, it can be seen that although all of the entire marble specimens experienced single shear fracture, the shear fracture angles (the angles between the shear fracture surfaces and the horizontal directions) depended on the confining pressure. At  $\sigma_3 = 2.5$  MPa, the shear fracture angle of marble was approximately  $68^\circ$ ; at  $\sigma_3 = 5.0$  MPa, the shear fracture angle of marble was approximately  $65^\circ$ ; at  $\sigma_3 = 7.5$  MPa, the shear fracture angle of marble was approximately  $60^\circ$ ; and at  $\sigma_3 = 10$  MPa, the shear fracture angle of marble was approximately  $57^\circ$ . The above analysis indicates that the shear fracture angle of marble under triaxial cyclic loading decreased gradually with increasing confining pressure.

Figure 15 shows the microscopic observation results of marble specimen after simple cyclic loading failure with respect to  $\sigma_3 = 2.5$  and 10 MPa. Compared with the microscopic observation results of marble specimen under triaxial monotonic loading failure shown in Fig. 7, it is clear that the damage to the marble specimen after triaxial cyclic loading failure was more serious, which agrees very well with the previous research results on sandstone specimen (Yang et al. 2015a). Furthermore, it should be noted that under higher confining pressures, near the main shear crack, the mineral grains also experienced more serious damage due to the following reason (Yang et al. 2016). Under lower confining pressures, the specimen failed mainly along the shear fracture plane, which was dominated by grain boundary cracks or transgranular cracks, whereas in other regions, most of the mineral grains were intact and no obvious grain boundary cracks and transgranular cracks were observed. However, under higher confining pressures, the mineral grains with low strengths and stiffnesses first reached maximum supporting capacity and experienced yield softening (Yang et al. 2008).

**Fig. 14** Ultimate failure mode of marble specimen under simple cyclic loading





**Fig. 15** Photomicrographs of marble specimen under simple cyclic loading

Afterward, if we want to cause the specimen to fail macroscopically, the axial deformation must be increased continuously. Thus, when the macroscopic stress–strain response of the tested marble reaches the peak strength, the mesoscopic grains with higher strengths and stiffnesses in the specimen will also reach their maximum supporting limits and experience yielding failure. Therefore, from Fig. 15b, we can observe a large amount of damage and failure of the mineral grains besides one main shear failure plane in the crystalline marble at  $\sigma_3 = 10$  MPa.

## 5 Triaxial Experimental Results of Marble Under Complex Cyclic Loading

In accordance with the path shown in Fig. 5, Fig. 16 illustrates the experimental results of marble specimens under complex cyclic loading. It should be noted that in Fig. 16, five specimens experience different axial strain values. For the same specimen, the stress level at point A was approximately equal to that at point B, but their axial strain values are different. The marble specimen with larger axial strain at point A indicates that the marble had a larger damage extent. In Fig. 16, the points A, B and C correspond to those shown in Fig. 5. After point C, the specimens had become damaged, and the axial deviatoric stress–axial strain curve of the damaged marble specimens at four different confining pressures can be also obtained. Furthermore, it can be seen from Fig. 16 that the five specimens had very small differences, which can be used to investigate the mechanical behavior of the marble compressed different deformation positions, as shown in Fig. 17. In Fig. 17, each axial deviatoric stress–axial strain curve of marble specimens is redrawn by adjusting the axial strain shown in Fig. 16 to the zero point. The corresponding elastic moduli and peak strengths of the damaged

marble specimens are listed in Tables 2 and 3, respectively. We can therefore analyze the effects of damaged extent on the peak strength and elastic modulus of the marble in detail.

### 5.1 Elastic Modulus of Marble Under Complex Cyclic Loading

Table 2 lists the elastic moduli of the marble specimens under complex cyclic loading. Based on the experimental data listed in Table 2, we can in detail investigate the variations in the elastic moduli of the marble specimens under complex cyclic loading, as shown in Figs. 18 and 19.

From Fig. 18, it can be seen that at  $\sigma_3 = 10$  MPa, the  $Es^B$  values of marble decreased gradually from 43.37 to 24.51 GPa as  $\varepsilon_{1A}$  increases from  $5.035 \times 10^{-3}$  to  $16.96 \times 10^{-3}$ . The variation in the  $Es^{4th}$  values of the marble with the axial deformation at point A was similar to that of  $Es^B$ , which also decreased from 37.27 to 23.76 GPa in the variation range of the same axial strain. This can be interpreted as follows. The marble specimen with larger compressed axial deformation suffered more damages in comparison with that of the specimen with less compressed axial deformation, which resulted in decrease in the  $Es^B$  or  $Es^{4th}$  values of the marble specimen with increasing compressed deformation. However, the  $Es^A$  values of the marble first decreased sharply from 40.25 to 34.85 GPa as  $\varepsilon_{1A}$  increased from  $5.035 \times 10^{-3}$  to  $7.958 \times 10^{-3}$ , and there were then no large variations from 34.85 to 31.37 GPa as  $\varepsilon_{1A}$  increases from  $7.958 \times 10^{-3}$  to  $16.96 \times 10^{-3}$ . Those behaviors can be explained as follows. When the marble specimen GL-A12<sup>#</sup> was loaded to point D, a local yielding failure occurred inside the specimen, and it was possible to strengthen the supporting structure of the specimen, which resulted in a relatively higher stiffness. Therefore, the  $Es^A$  value of the marble at



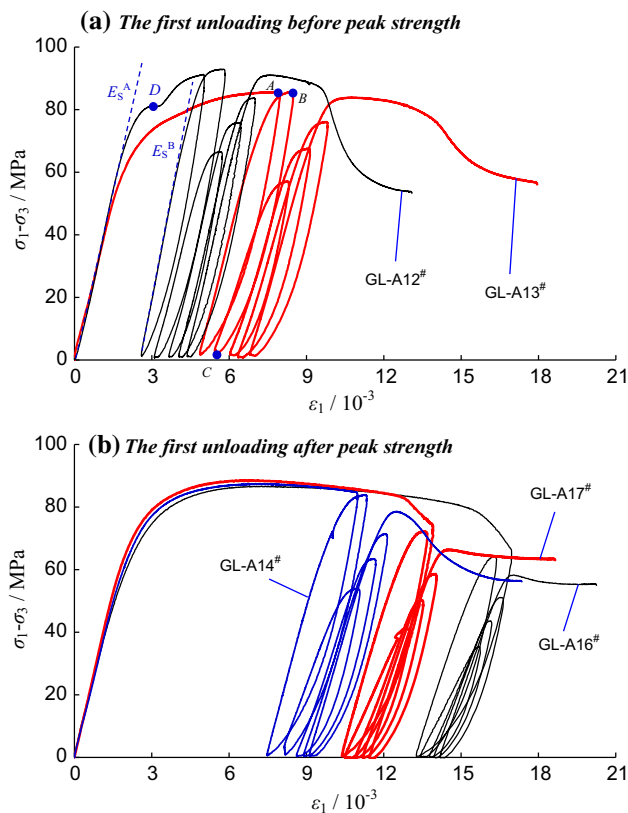


**Fig. 16** Experimental results of marble specimens under complex cyclic loading in accordance with the path shown in Fig. 4

$\epsilon_{1A} = 5.035 \times 10^{-3}$  was obviously higher than those for the other four various axial strain values. However, the  $E_s^A$  values of the marble at the other four various axial strain values were approximately equal, which shows the good consistency of the four tested specimens.

However, it should be noted that in all cases, the  $E_s^{4th}$  values of the marble were lower than the  $E_s^B$  values even though the confining pressures were all 10 MPa, but the difference between  $E_s^{4th}$  and  $E_s^B$  decreased with the increase in axial deformation at point A, as shown in Fig. 18b. The above description indicates that the loading history after point C shown in Fig. 16 greatly affected the elastic modulus of the marble and the effect decreased as the compressed axial deformation increased. When the marble was compressed to  $16.96 \times 10^{-3}$  at point A, the specimen almost supported the axial capacity by friction slippage, as shown in Fig. 16b. Therefore, the loading history had almost no any effect on the elastic modulus of the marble, which can be inferred from approximate elastic modulus of the marble at  $\epsilon_{1A} = 16.96 \times 10^{-3}$ .

Figure 19 shows the effects of confining pressure and axial strain at point A on the elastic modulus of marble specimen under complex cyclic loading. From Fig. 19a, it can be seen that for the same axial strain at point A, the elastic modulus of damaged marble specimen increased

nonlinearly with the increase in confining pressure, which can be expressed by the equation:  $E_s = a \times \sigma_3^b$ .  $a$  and  $b$  are both material parameters, which were determined according to the experimental results. Furthermore, the elastic modulus of marble increased more and more slowly with increasing confining pressure. However, from Fig. 19b, it is clear that for the same confining pressure, the elastic modulus of the damaged marble specimen decreased nonlinearly with the increase in axial strain at point A, which can be expressed by the equation:  $E_s = c \times \epsilon_{1A}^{-d}$ .  $c$  and  $d$  are both material parameters, which were determined according to the experimental results. Furthermore, the elastic modulus of the marble decreased more and more slowly with increasing axial strain at point A.

### 5.2 Peak Strength of Marble Under Complex Cyclic Loading

Figure 20 shows peak strength behavior of the marble specimens compressed to different deformation positions, which were obtained according to the experimental results shown in Fig. 17. From Fig. 20, we can see that the peak strength of marble changed with different axial deformation positions at point A. At the same confining pressure, the peak strength of marble specimen decreased with the increase in axial strain at point A. For example, at  $\sigma_3 = 2.5$  MPa, the peak strength of marble specimen decreased from 66.53 to 35.36 MPa as the axial strain at point A increased from  $5.035 \times 10^{-3}$  to  $16.96 \times 10^{-3}$ , which was a result of the gradual increase in damage extent with the axial deformation. For the same strain at point A, the peak strength of marble specimen increased with the confining pressure, which could be well expressed by the linear Mohr–Coulomb criterion. By using Eq. (1), we confirmed the cohesions and internal friction angles of the marble specimens for different axial strain values, all of which are listed in Table 3. In accordance with the cohesions and internal friction angles (Table 3), the effect of the axial strain at point A on the strength parameters of marble specimen under complex cyclic loading can be analyzed.

Figure 21 plots the relationship between axial strain at point A and the strength parameters of marble specimen under complex cyclic loading. In the case of the variation in cohesion with increasing axial strain at point A, the cohesion of marble decreased gradually from 14.28 to 6.97 MPa with increasing axial strain at point A. However, the attenuating extent was different, and the cohesion of the marble decreased rapidly at the beginning and was then followed by a slow attenuation, which can be well expressed by the power function relation  $C = 38.1 \times \epsilon_{1A}^{-0.578}$ , for which the correlation coefficient of the nonlinear regression was approximately 0.954, as evidenced by Fig. 21a. However, when compared with the

**Fig. 17** Axial deviatoric stress–strain curve of marble specimens compressed to different deformation positions

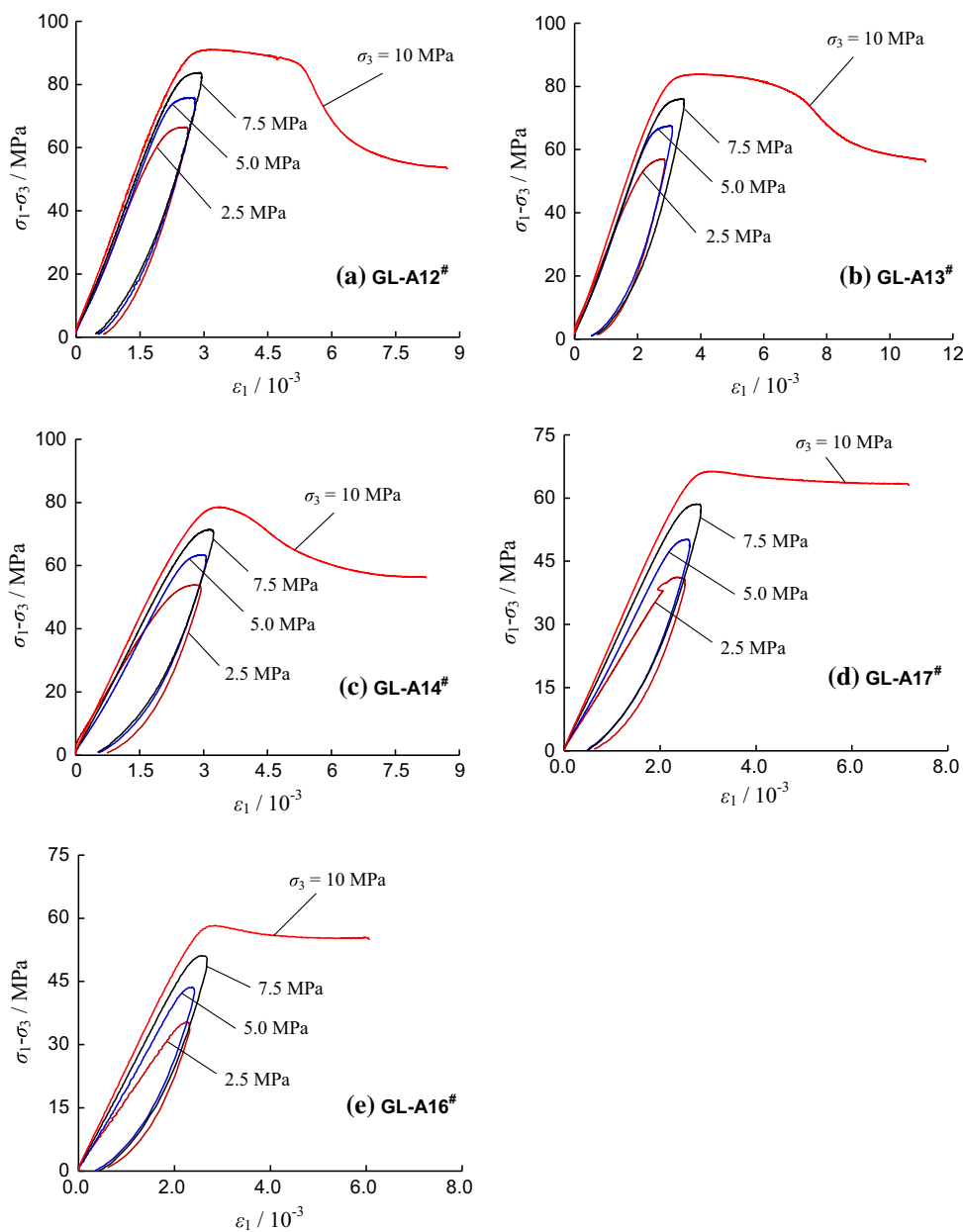


**Table 2** Elastic modulus of marble under complex cyclic loading (unit: GPa)

Specimen	$\epsilon_{1A}$ ( $10^{-3}$ )	$E_S^A$ (GPa) ( $\sigma_3 = 10$ MPa)	$E_S^B$ (GPa) ( $\sigma_3 = 10$ MPa)	$E_S^{1st}$ (GPa) ( $\sigma_3 = 2.5$ MPa)	$E_S^{2nd}$ (GPa) ( $\sigma_3 = 5.0$ MPa)	$E_S^{3rd}$ (GPa) ( $\sigma_3 = 7.5$ MPa)	$E_S^{4th}$ (GPa) ( $\sigma_3 = 10$ MPa)
GL-A12#	5.035	40.25	43.37	34.20	35.70	36.77	37.27
GL-A13#	7.958	34.85	33.60	25.13	29.06	29.15	30.12
GL-A14#	10.98	33.99	30.82	22.52	26.19	27.10	28.28
GL-A17#	13.92	36.12	27.98	18.72	22.82	24.57	26.06
GL-A16#	16.96	31.37	24.51	16.53	20.37	22.07	23.76

$E_S$  represents the elastic modulus of rock, which is confirmed according to the slope of elastic deformation stage. The elastic modulus of marble at point A and B is denoted in Fig. 16. The four stages of marble under four different confining pressures are denoted in Fig. 5

**Fig. 18** Elastic modulus of marble specimen at various deformation positions ( $\sigma_3 = 10$  MPa)

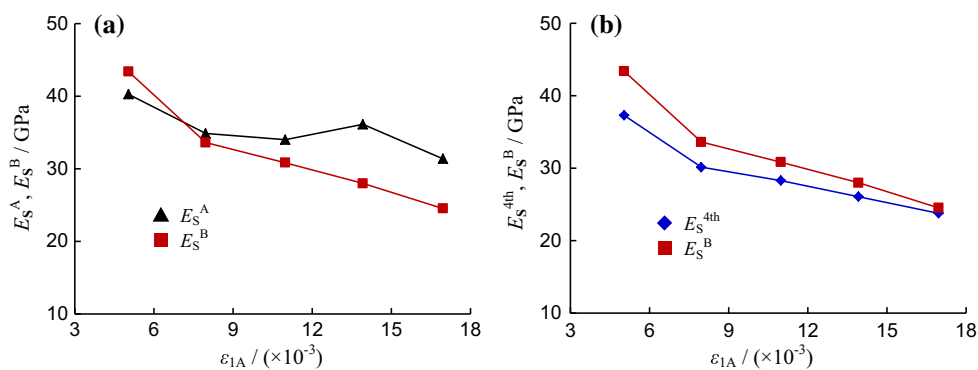


**Fig. 19** Effect of confining pressure and axial strain at point A on elastic modulus of marble specimen under complex cyclic loading

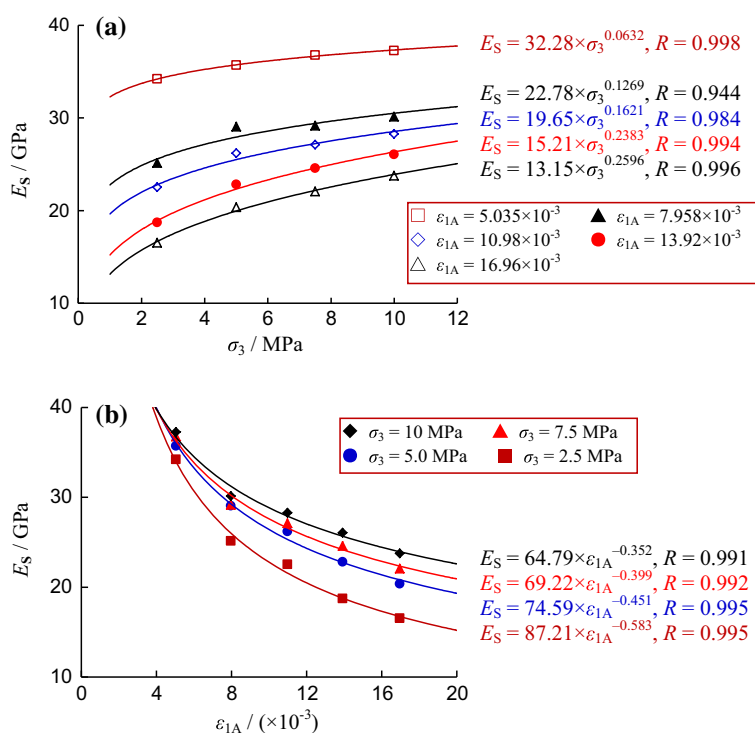


**Fig. 20** Peak strength behavior of marble specimens compressed to different deformation positions

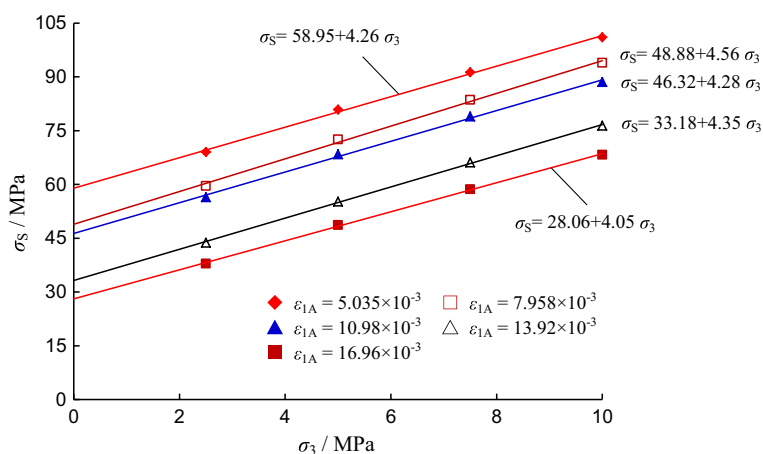
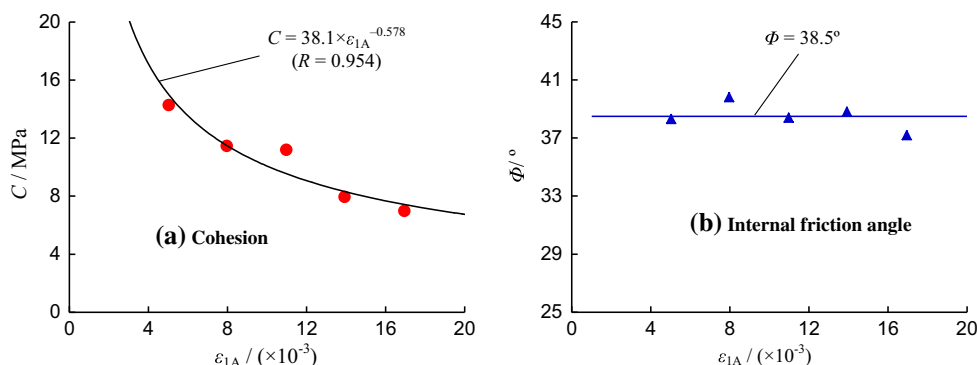


**Table 3** Triaxial strength of marble under complex cyclic loading (unit: MPa)

Specimen	$\epsilon_{1A} (10^{-3})$	$\epsilon_{1B} (10^{-3})$	$\sigma_3 = 2.5 \text{ MPa}$	$\sigma_3 = 5 \text{ MPa}$	$\sigma_3 = 7.5 \text{ MPa}$	$\sigma_3 = 10 \text{ MPa}$	$C \text{ (MPa)}$	$\Phi \text{ (}^\circ\text{)}$
GL-A12 <sup>#</sup>	5.035	5.842	66.53	75.89	83.76	91.06	14.28	38.3
GL-A13 <sup>#</sup>	7.958	8.444	57.05	67.55	76.09	83.90	11.45	39.8
GL-A14 <sup>#</sup>	10.98	11.27	53.91	63.41	71.44	78.59	11.19	38.4
GL-A17 <sup>#</sup>	13.92	13.51	41.26	50.22	58.61	66.38	7.95	38.8
GL-A16 <sup>#</sup>	16.96	16.38	35.36	43.67	51.11	58.28	6.97	37.2

The triaxial strength of marble listed in this table is obtained according to the experimental results shown in Fig. 16

**Fig. 21** Effect of axial strain at point A on the strength parameters of marble specimen under complex cyclic loading



cohesion, the internal friction angle of the marble was relatively insignificant with the axial strain (point A) region considered here, as shown in Fig. 21b. The internal friction angle of marble at various axial strain values ranged from 37.2° to 39.8°, and the average value was approximately 38.5°. Therefore, complex cyclic loading caused some damage to the marble specimens, which can be interpreted as losses in specimens' cohesions.

Compared with the cohesion of the marble under triaxial monotonic loading (11.77 MPa), only the cohesion of the marble at  $\epsilon_{1A} = 5.035 \times 10^{-3}$  was relatively higher (14.28 MPa), primarily because the tested marble specimen GL-A12<sup>#</sup> had a relatively higher supporting capacity than that used under triaxial monotonic loading, as shown in Fig. 16a. Afterward, it can be seen that cohesion of marble specimen at  $\epsilon_{1A} = 7.958 \times 10^{-3}$  and  $10.98 \times 10^{-3}$  was all approximately equal to those under triaxial monotonic loading because the specimen experienced minor damage after being loaded to the corresponding strain at point A. However, the cohesions of the marble specimen at  $\epsilon_{1A} = 13.92 \times 10^{-3}$  and  $16.96 \times 10^{-3}$  were all obviously lower than those under triaxial monotonic loading due to the serious damage experienced by the specimen when being loaded to the corresponding strain at point A. However, the internal friction angles of the marble specimens under complex cyclic loading were all approximately equal to those under triaxial monotonic loading (approximately 40.9°), which means that the damage extent had an

insignificant effect on the internal friction angle of the marble, as evidenced by Fig. 21b.

To describe the peak strength characteristics of the marble specimens under complex cyclic loading and various deformation positions, a revised strength criterion for damaged rocks is put forward on the basis of the linear Mohr–Coulomb criterion:

$$\begin{aligned} \sigma_S^* &= \frac{2C^* \cos k\varphi_0 + \sigma_3(1 + \sin k\varphi_0)}{1 - \sin k\varphi_0} \\ &= \frac{2mC_0\epsilon_{1A}^{-n} \cos k\varphi_0 + \sigma_3(1 + \sin k\varphi_0)}{1 - \sin k\varphi_0} \end{aligned} \quad (3)$$

where  $C^*$  is the cohesion of damaged marble, which depends on various damage extents, and is equal to  $mC_0\epsilon_{1A}^{-n}$ , where  $C_0$  is the cohesion of undamaged marble, which was confirmed in the triaxial monotonic loading test in this research to be 11.77 MPa,  $\varphi_0$  is the internal friction angle of undamaged marble, which was 40.9° in this research, and  $k$  is a coefficient, obtained by the ratio of the average value of damaged marbles to  $\varphi_0$  and was equal to 0.94.

Figure 22 illustrates the ultimate failure modes of the marble specimens under complex cyclic loading. From Fig. 22, it is clear that all the marble specimens under complex cyclic loading exhibited typical shear failure modes with a single shear fracture plane. Furthermore, the angles of the shear fracture planes were all approximately 60°.

Figure 23 shows the microscopic observation results of marble specimen after complex cyclic loading failure with



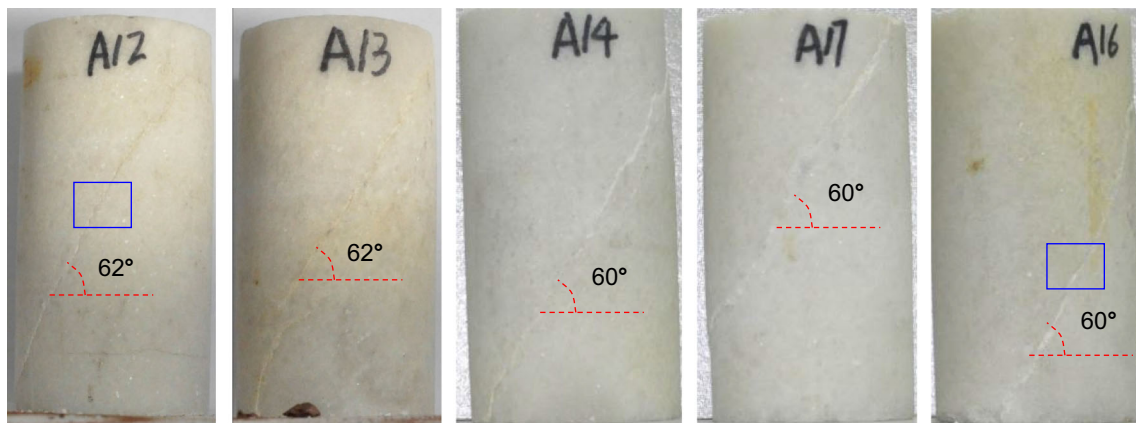


Fig. 22 Ultimate failure modes of marble specimens under complex cyclic loading

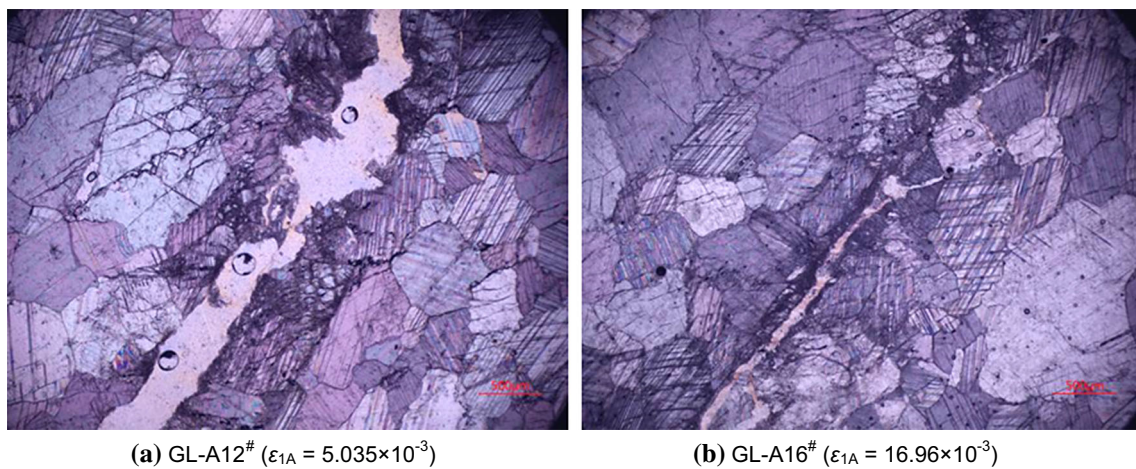


Fig. 23 Photomicrographs of marble specimen under complex cyclic loading

respect to different axial deformation value. Compared with the microscopic observation results of marble specimen under simple cyclic loading failure shown in Fig. 15, it is clear that the damage of marble specimen after complex cyclic loading failure was more serious, which indicates that complex loading path can lead to more obvious damage on the rock specimen. From Fig. 23, it can be seen that main shear failure is very obvious, but nearby the main shear failure, many grains suffered serious damage.

### 6 Conclusions

This paper explored the mechanical damage characteristics of crystalline marble using a series of triaxial monotonic and cyclic experiments. Photomicrographs of marble specimens after triaxial monotonic and cyclic loading are simultaneously captured to deeply reveal the deformation failure mechanism of marble. Based on the experimental results, the following conclusions can be drawn:

1. Under triaxial monotonic loading, the post-peak deformation of the tested marble changed gradually from strain softening to strain hardening as  $\sigma_3$  increased from 0 to 10 MPa. Under uniaxial compression, the marble specimen showed brittle failure characteristics, with some axial splitting tensile cracks; in the range of  $\sigma_3 = 2.5\text{--}7.5$  MPa, the marble specimen took on single shear fracture characteristics, with a larger fracture angle of approximately  $65^\circ$ , but at  $\sigma_3 = 10$  MPa, the marble specimen did not have an obvious shear fracture surface. The triaxial cyclic experimental results indicate that in the range of tested confining pressures, the triaxial strengths of the marble specimens under cyclic loading were approximately equal to those under monotonic loading. Although there was only one single shear fracture, the fracture angle of marble under triaxial cyclic loading decreased gradually with increasing  $\sigma_3$ .
2. On the basis of the experimental results of the marble under triaxial cyclic loading, it can be seen that at the

same confining pressure, the plastic deformation of the marble increased slowly with the increase in unloading stress level, whereas after the peak strength, the plastic deformation of marble increased dramatically even with the reduction in unloading stress level. With the increase in cycle number, the elastic strain of marble at first all increased and then decreased, having a maximum value, but the plastic strain of marble increased nonlinearly. To quantitatively evaluate the damage extent of the marble specimen under triaxial cyclic loading, a damage variable was defined in accordance with the irreversible deformation for each cycle. Furthermore, the evolution characteristics of Young's modulus of marble under triaxial cyclic loading were evaluated.

- Under complex cyclic loading, the peak strength of marble changed with different axial deformation positions at point A. At the same confining pressure, the peak strength of marble specimen decreased with the increase in axial strain at point A, which was a result of the gradual increase in damage extent with the axial deformation. For the same axial strain at point A, the peak strength of marble specimen increased with the confining pressure, which could be well expressed by the linear Mohr–Coulomb criterion. The cohesion of marble attenuated following a power function relation with the increase in axial strain at point A, whereas the internal friction angle of marble under complex cyclic loading path was not dependent on axial strain at point A. For the damaged specimen, the elastic modulus of marble increased nonlinearly with the confining pressure. To describe the peak strength characteristics of marble specimens under complex cyclic loading with various deformation positions, a revised strength criterion for damaged rocks was put forward on the basis of the linear Mohr–Coulomb criterion.

**Acknowledgements** This research was supported by the Fundamental Research Funds for the Central Universities (2015XKZD05). The authors would like to express their sincere gratitude to the editor and the anonymous reviewers for their valuable comments, which have greatly improved this paper.

## References

- Akesson U, Hansson J, Stigh J (2004) Characterisation of microcracks in the Bohus granite, western Sweden, caused by uniaxial cyclic loading. *Eng Geol* 72:131–142
- Bagde MN, Petros V (2005) The effect of machine behavior and mechanical properties of intact sandstone under static and dynamic uniaxial cyclic loading. *Rock Mech Rock Eng* 38(1):59–67
- Cheng Y, Wong LNY, Maruvanchery V (2016) Transgranular crack nucleation in Carrara marble of brittle failure. *Rock Mech Rock Eng* 49:3069–3082
- Erarslan N, Williams DJ (2012) Investigating the effect of cyclic loading on the indirect tensile strength of rocks. *Rock Mech Rock Eng* 45:327–340
- Heap MJ, Baud P, Meredith PG, Bell AF, Main IG (2009a) Time-dependent brittle creep in Darley Dale sandstone. *J Geophys Res*. doi:10.1029/2008JB006212
- Heap MJ, Vinciguerra S, Meredith PG (2009b) The evolution of elastic moduli with increasing crack damage during cyclic stressing of a basalt from Mt. Etna volcano. *Tectonophysics* 47:153–160
- Jafari MK, Hosseini KA, Pellet F, Boulon M, Buzzi O (2003) Evaluation of shear strength of rock joints subjected to cyclic loading. *Soil Dyn Earthq Eng* 23:619–630
- Liu JF, Xie HP, Hou ZM, Yang CH, Chen L (2014) Damage evolution of rock salt under cyclic loading in uniaxial tests. *Acta Geotech* 9:153–160
- Migliazza M, Ferrero AM, Spagnoli A (2011) Experimental investigation on crack propagation in Carrara marble subjected to cyclic loads. *Int J Rock Mech Min Sci* 48:1038–1044
- Pei JL, Fei WP, Liu JF (2016) Spatial evolution and fractal characteristics of natural fractures in marbles under uniaxial compression loading based on the source location technology of acoustic emission. *Environ Earth Sci* 75:828
- Qiu SL, Feng XT, Xiao JQ, Zhang CQ (2014) An experimental study on the pre-peak unloading damage evolution of marble. *Rock Mech Rock Eng* 47:401–419
- Rao MVMS, Ramana YV (1992) A study of progressive failure of rock under cyclic loading by ultrasonic and AE monitoring techniques. *Rock Mech Rock Eng* 25(4):237–251
- Trippetta F, Collettini C, Meredith PG, Vinciguerra S (2013) Evolution of the elastic moduli of seismogenic Triassic Evaporites subjected to cyclic stressing. *Tectonophysics* 592:67–79
- Wang ZC, Li SC, Qiao LP, Zhao JG (2013) Fatigue behavior of granite subjected to cyclic loading under triaxial compression condition. *Rock Mech Rock Eng* 46:1603–1615
- Xiao JQ, Ding DX, Jiang FL, Xu G (2010) Fatigue damage variable and evolution of rock subjected to cyclic loading. *Int J Rock Mech Min Sci* 47:461–468
- Xu T, Tang CA, Zhao J, Li LC, Heap MJ (2012) Modelling the time-dependent rheological behavior of heterogeneous brittle rocks. *Geophys J Int* 189(3):1781–1796
- Yang SQ, Jing HW (2013) Evaluation on strength and deformation behavior of red sandstone under simple and complex loading paths. *Eng Geol* 154:1–17
- Yang SQ, Jiang YZ, Xu WY, Chen XQ (2008) Experimental investigation on strength and failure behavior of pre-cracked marble under conventional triaxial compression. *Int J Solids Struct* 45:4796–4819
- Yang SQ, Jing HW, Li YS, Han LJ (2011) Experimental investigation on mechanical behavior of coarse marble under six different loading paths. *Exp Mech* 51:315–334
- Yang SQ, Jing HW, Cheng L (2014) Influences of pore pressure on short-term and creep mechanical behavior of red sandstone. *Eng Geol* 179:10–23
- Yang SQ, Ranjith PG, Huang YH, Yin PF, Jing HW, Gui YL, Yu QL (2015a) Experimental investigation on mechanical damage characteristics of sandstone under triaxial cyclic loading. *Geophys J Int* 201(2):662–682
- Yang SQ, Xu P, Ranjith PG, Chen GF, Jing HW (2015b) Evaluation of creep mechanical behavior of deep-buried marble under triaxial cyclic loading. *Arab J Geosci* 8:6567–6582
- Yang SQ, Ju Y, Gao F, Gui YL (2016) Strength, deformability and X-ray micro-CT observations of deeply buried marble under different confining pressures. *Rock Mech Rock Eng* 49(11):4227–4244

- Zhou XP, Zhang XQ (2017) The 3D numerical simulation of damage localization of rocks using general particle dynamics. *Eng Geol* 224:29–42
- Zhou XP, Xia EM, Yang HQ, Qian QH (2012) Different crack sizes analyzed for surrounding rock mass around underground caverns in Jinping I hydropower station. *Theoret Appl Fract Mech* 57:19–30
- Zhu WC, Li ZH, Zhu L, Tang CA (2010) Numerical simulation on rockburst of underground opening triggered by dynamic disturbance. *Tunn Undergr Space Technol* 25(5):587–599